

Development of ultra-fine grained W–TiC and their mechanical properties for fusion applications

H. Kurishita ^{a,*}, Y. Amano ^b, S. Kobayashi ^b, K. Nakai ^b, H. Arakawa ^a,
Y. Hiraoka ^c, T. Takida ^d, K. Takebe ^d, H. Matsui ^a

^a International Research Center for Nuclear Materials Science, Institute for Materials Research (IMR),
Tohoku University, Oarai, Ibaraki 311-1313, Japan

^b Department of Materials Science and Engineering, Ehime University, Matsuyama 790-8577, Japan

^c Okayama University of Science, 1-1 Ridai-cho, Okayama 700-0005, Japan

^d A.L.M.T. Corp., 2 Iwase-koshi-machi, Toyama 931-8371, Japan

Abstract

Effects of neutron irradiation on microstructural evolution and radiation hardening were examined for fine-grained W–0.3 wt%TiC (grain size of 0.9 μm) and commercially available pure W (20 μm). Both materials were neutron irradiated at 563 K to 9×10^{23} n/m² ($E > 1$ MeV) in the Japan Materials Testing Reactor (JMTR). Post-irradiation examinations showed that the microstructural changes and the degree of hardening due to irradiation were significantly reduced for fine-grained W–0.3TiC compared with pure W, demonstrating the significance of grain refinement to improve radiation resistance. In order to develop *ultra-fine* grained W–TiC compacts with nearly full densification, the fabrication process was modified, so that W–(0.3–0.7)%TiC with 0.06–0.2 μm grain size and 99% of relative density was fabricated. The achievable grain refinement depended on TiC content and milling atmosphere. The three-point bending fracture strength at room temperature for ultra-fine grained W–TiC compacts of powder milled in H₂ reached approximately 1.6–2 GPa for composition near 0.5%TiC.

© 2007 Elsevier B.V. All rights reserved.

1. Introduction

Tungsten and its alloys are very promising for use as high heat flux components and high-power density structural materials in radiation environments because of their excellent compatibility with liquid metals, high melting points, low thermal expansion coefficients and low sputtering yield,

etc. However, they exhibit serious embrittlement in several regimes, i.e., low temperature embrittlement, recrystallization embrittlement and radiation embrittlement [1]. In order to alleviate such embrittlement, the authors have been developing tungsten alloys with a microstructure of fine grains and finely dispersed particles of transition metal carbides such as TiC by applying mechanical alloying (MA) [2] and hot isostatic pressing (HIP), followed by hot forging and hot rolling [3–6].

Our recent studies on low temperature embrittlement in MA-HIPed W–TiC alloys showed that the

* Corresponding author. Tel.: +81 29 267 4157; fax: +81 29 267 4947.

E-mail address: kurishi@imr.tohoku.ac.jp (H. Kurishita).

beneficial effect of plastic working such as forging and rolling after consolidation on room-temperature ductility improvement is strongly dependent on grain size and magnified with decreasing grain size [6]. This indicates the significance of further grain refinement for ductility enhancement. In addition, recent experimental and simulation studies of radiation effects on fine/refined/nanocrystalline materials [7–19] showed that these structures are effective in improving radiation resistance. However, there have been no reports on the effect of grain refinement on radiation resistance for W and its alloys.

In this study MA-HIPed W–0.3%TiC with a grain size of 0.9 μm and commercially available pure W specimens (grain size: 20 μm) were irradiated with fast neutrons in the Japan Materials Testing Reactor (JMTR) and their microstructural evolution and Vickers microhardness were examined and compared. In order to achieve *further* refinement of the W–TiC compacts with nearly full densification the fabrication process has been modified. It is demonstrated that W–(0.3–0.7)% TiC compacts with ultra-fine grains of 0.06–0.2 μm and a high relative density of 99% have been successfully fabricated. The current status of the microstructural and mechanical property evaluation for the ultra-fine grained W–TiC compacts is presented.

2. Experimental

Powders of pure W (an average particle size 4.0 μm and purity 99.9%) and TiC (40 μm , 99.9%) were used as the starting materials. They were mixed in a glove box to provide nominal compositions of pure W and W–(0.3–0.7)wt%TiC and then charged into two vessels made of TZM (Mo–0.5%Ti–0.1%Zr alloy) together with TZM balls for MA. MA treatments were conducted by a 3MPDA (three mutually perpendicular directions agitation) ball mill in a purified Ar (purity 99.9999%) or purified H₂ gas atmosphere. The details of MA processes are reported elsewhere [5,6].

The MA treated powder was placed in a Mo boat and heated at 1073 K for 3.6 ks in vacuum to remove Ar or H₂ introduced during MA process. The vacuum-treated powder was charged into a mild steel capsule and then subjected to HIP in an Ar atmosphere at first at 1620 K and 200 MPa for 3 h, with in some cases an additional HIP at 2220 K and 200 MPa for 3 h for the sintered compact. The measured relative densities of the as-

HIPed compacts were approximately 99%. The contents of oxygen and nitrogen impurities were approximately 200–400 and 60–100 wt ppm, respectively. Mo contents arising from the vessels and balls of TZM during MA were in a range between 1.8 and 2.4 wt%.

The as-HIPed compacts were machined to prepare specimens for microstructural observation by transmission electron microscopy (TEM) and Vickers microhardness and three-point bending (3PB) tests. TEM observations were made with a JEM-2000FX or JEM-4000FX operating at 200 or 400 kV, respectively. Vickers microhardness was measured at room temperature with a load of 4.9 N for 20 s. 3PB tests were conducted on miniaturized specimens with dimensions of 1 mm by 1 mm by 20 mm with a span of 13.3 mm and a crosshead speed of 0.01 mm s⁻¹. Fracture surfaces of the tested specimens were examined with a field emission scanning electron microscope.

Neutron irradiation of TEM disk specimens of two-step HIPed W–0.3TiC (grain size: 0.9 μm) and commercially available pure W in the stress relieved state (20 μm) was performed at 563 K to 9×10^{23} n/m² ($E > 1$ MeV) in JMTR. Post-irradiation examinations (PIE) were conducted in the facilities of IMR-Oarai center, Tohoku University.

3. Results and discussion

3.1. Neutron irradiation effect

TEM observations of pure W and W–0.3TiC compacts showed a high density of sub-grain boundaries. The average diameters of sub-grains before and after irradiation were 0.71 μm and 0.74 μm for pure W and 0.49 μm and 0.53 μm for W–0.3TiC, respectively. The sub-grain sizes for both materials are in a similar range, while the grain sizes exhibit a rather large difference (W: 20 μm , W–0.3TiC: 0.9 μm).

Fig. 1 shows bright-field and dark-field images and a selected area diffraction pattern from a dispersoid existing at a grain boundary in neutron irradiated W–0.3TiC. From the pattern the dispersoid was identified to be TiC, although it may be Ti(C, O, N)_x. It was found that a Kurdjumov–Sachs (K–S) orientation relationship exists between the TiC dispersoid and the W matrix. The K–S relationship meets

$$(111)_{\text{fcc}} \parallel (110)_{\text{bcc}}, [1\bar{1}0]_{\text{fcc}} \parallel [1\bar{1}1]_{\text{bcc}}.$$

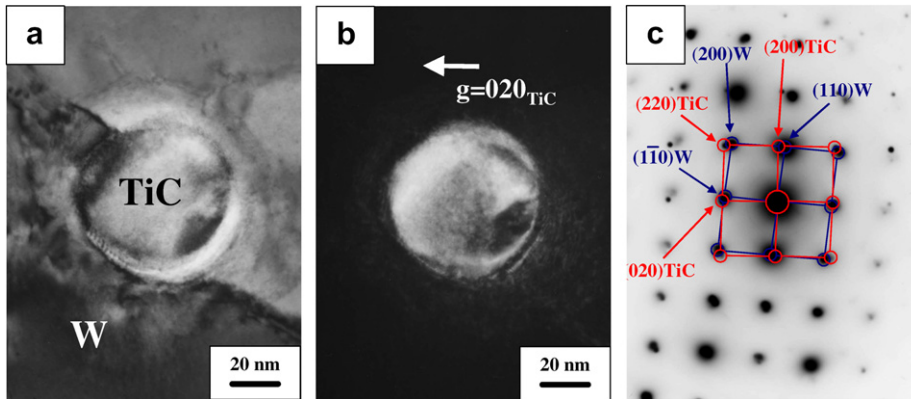


Fig. 1. (a) Bright-field and (b) dark-field images and (c) a selected area diffraction pattern from a dispersoid existing at a grain boundary in neutron irradiated W-0.3TiC.

Such a good orientation relationship between the TiC dispersoid and the W matrix indicates that the TiC dispersoid was formed by precipitation from a supersaturated state. Since the precipitation is difficult to occur at a low irradiation temperature of 563 K ($T/T_m = 0.15$, where T_m is the melting point of W), the observed TiC dispersoid was not formed as a consequence of irradiation, but already existed in the original microstructure. In fact, such TiC dispersoids were observed at grain boundaries before irradiation. This demonstrates that the TiC dispersoids are stable against neutron irradiation under the present conditions.

Fig. 2 shows TEM microstructures near a grain boundary for (a) pure W and (b) W-0.3TiC after neutron irradiation. A number of radiation induced defects such as small black dots or interstitial-type dislocation loops are observed in the grain interior. Fig. 2(c) shows the size (radius) distribution of radi-

ation-induced defects in pure W and W-0.3TiC. The average radius and number density of the defects were 3.3 nm and $3600/\mu\text{m}^3$ for pure W and 2.9 nm and $2700/\mu\text{m}^3$ for W-0.3TiC, respectively. MA in an Ar atmosphere resulted in the formation of nano-sized Ar cavities (W-0.3TiC [6]), which may cause overestimation of the defect density. W-0.3TiC likely contains fewer radiation-induced defects and hence exhibits higher resistance to radiation-induced microstructural changes than pure W. This suggests that the sink efficiency of grain boundaries and TiC dispersoids is higher than that of sub-grain boundaries.

The Vickers microhardness numbers before and after irradiation were measured to be 506 and 569 for pure W and 667 and 697 for W-0.3TiC. The amount of radiation hardening, ΔH_V , 30 for W-0.3TiC and 63 for pure W, was much less for W-0.3TiC. These results indicate that the fine-

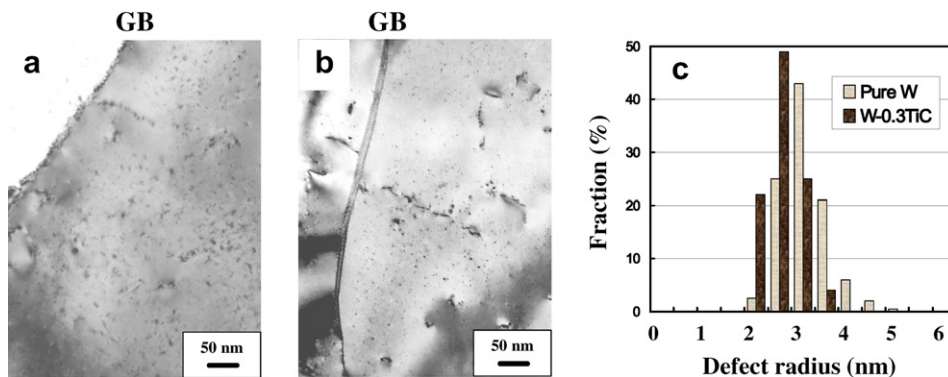


Fig. 2. TEM bright-field images near a grain boundary for (a) pure W and (b) fine-grained W-0.3TiC compacts after neutron irradiation at 563 K and (c) size distribution of radiation-induced defects.

grained, TiC dispersed microstructure in W–0.3TiC is effective in improving the resistance to radiation hardening.

3.2. Fabrication of ultra-fine grained W–TiC compacts

Fabrication of ultra-fine grained W–TiC compacts requires HIPing at lower temperatures to suppress grain growth. As the HIPing temperature is lowered, however, the densification of the compacts is inadequate; e.g., the relative density of a compact HIPed at 1350 °C is ~94%, whereas the grain size is as small as 50 nm [3]. Therefore, the fabrication process was modified to achieve a high relative density of ~99% in ultra-fine grained W–TiC. The modified process lead to the fabrication of consolidated bodies with a relative density of approximately 99%.

Table 1 lists the average grain sizes of pure W and W–TiC with different TiC additions and MA atmospheres. It is obvious that TiC addition and MA in Ar have a significant grain refinement effect. Larger grains of pure W are due to the absence of dispersed particles. Fig. 3 shows a TEM micrograph for W–0.7TiC (MA in Ar) exhibiting the smallest grain size. It was confirmed that Ar formed small bubbles or cavities in the compacts providing that MA was processed in Ar. Such bubbles or cavities may give a pinning effect similar to dispersoids and cause grain refinement.

Fig. 4 shows the dependence of 3PB fracture strength on TiC content and milling atmosphere. The fracture strength was estimated to be the maximum fiber stress given by

$$\sigma = 3PL/2Bt^2. \quad (1)$$

Here, σ is the stress, P is the applied load, L is the span (13.3 mm), B and t are the specimen width and thickness, respectively. MA in H₂ provides considerably higher fracture strength than that in Ar. This is likely attributed to easier removal of H₂ than that of Ar from the W–TiC compacts. The fracture strength of W–TiC with MA in H₂ reaches approx-

Table 1

Average grain sizes of pure W and W–TiC compacts with different TiC contents and milling atmospheres

MA atmosphere	Pure W	W–0.3TiC	W–0.5TiC	W–0.7TiC
Purified H ₂	3300	148	129	106
Purified Ar	–	–	79	59

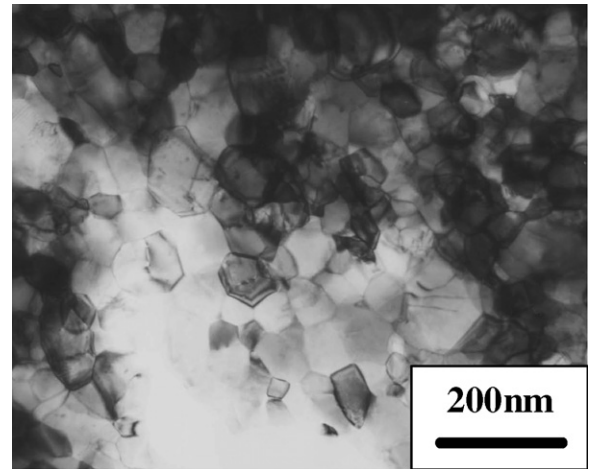


Fig. 3. A TEM bright-field image showing the grain structure of a HIPed W–0.7%TiC compact processed with MA in an Ar atmosphere.

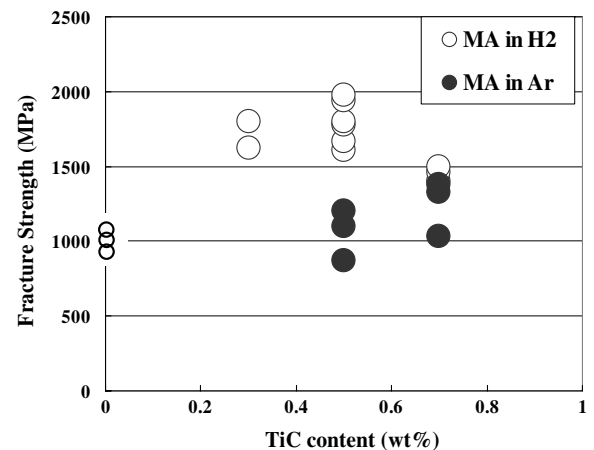


Fig. 4. 3PB fracture strength for pure W and W–TiC compacts with different TiC contents and milling atmospheres.

imately 1.6–2 GPa around 0.5%TiC. It should be noted that this value was obtained for the ultra-fine grained, as-HIPed W–0.5TiC compacts without anisotropy and is much higher than that for fine-grained W–0.3TiC with grain size of 0.6 μm, 1.2 GPa [6]. Pure W, on the other hand, although processed with MA in H₂, exhibited intergranular fracture at very low stresses, ~1000 MPa, which are much lower than the fracture strengths of W–TiC. The high strength of ultra-fine grained W–TiC is therefore attributable to grain-boundary strengthening by TiC dispersoids and to the reduction of the effective size of a weak grain boundary acting as a crack initiator by grain refinement.

4. Conclusions

- (1) Microstructural changes and radiation hardening by neutron irradiation at 563 K to 9×10^{23} n/m² ($E > 1$ MeV) in JMTR are significantly reduced for fine-grained W–0.3TiC with grain size of 0.9 μm compared with commercially available pure W with grain size of 20 μm .
- (2) TiC dispersoids at grain boundaries have a K–S orientation relationship with the W matrix and are stable against neutron irradiation under the present conditions.
- (3) Ductility enhancement and neutron irradiation resistance improvement for P/M W–TiC alloys require further grain refinement from fine grains to ultra-fine grains.
- (4) TiC additions up to 0.7 wt% and MA in an Ar atmosphere give a significant grain refinement effect due to the pinning effects of TiC dispersoids and Ar bubbles or cavities, resulting in the smallest grain size of 59 nm.
- (5) MA in H₂ provides considerably higher fracture strengths than that in Ar. The 3PB fracture strength at room temperature for ultra-fine grained W–(0.3–0.7)%TiC with MA in H₂ reaches approximately 1.6–2 GPa around 0.5%TiC content. These values are much higher than those for as-HIPed, fine-grained W–0.3TiC with a grain size of 0.6 μm , ~ 1.2 GPa.
- (6) The high strength of ultra-fine grained W–TiC is most likely due to grain-boundary strengthening by TiC dispersoids and to the reduction of the effective size of a weak grain boundary acting as a crack initiator by grain refinement.

Acknowledgement

The authors would like to express their gratitude to Dr S. Matsuo for his review. He present work was partly supported by a Grant-in-Aid for Scien-

tific Research (A) (#13308022), Japan Society for the Promotion of Science (JSPS), which is greatly appreciated.

References

- [1] For instance I. Smid, M. Akiba, G. Vieider, L. Plöchl, *J. Nucl. Mater.* 253–263 (1998) 160.
- [2] J.S. Benjamin, *Metall. Trans.* 5 (1970) 2943.
- [3] Y. Kitsunai, H. Kurishita, M. Narui, H. Kayano, Y. Hiraoka, T. Igarashi, T. Takida, *J. Nucl. Mater.* 271&272 (1999) 423.
- [4] H. Kurishita, Y. Kitsunai, T. Kuwabara, M. Hasegawa, Y. Hiraoka, T. Takida, T. Igarashi, *J. Plasma Fus. Res.* 75 (1999) 594 (in Japanese).
- [5] Y. Ishijima, H. Kurishita, K. Yubuta, H. Arakawa, M. Hasegawa, Y. Hiraoka, T. Takida, K. Takebe, *J. Nucl. Mater.* 329–333 (2004) 75.
- [6] Y. Ishijima, H. Kurishita, H. Arakawa, M. Hasegawa, Y. Hiraoka, T. Takida, K. Takebe, *Mater. Trans.* 46 (2005) 568.
- [7] H. Kurishita, Y. Kitsunai, T. Shibayama, H. Kayano, Y. Hiraoka, *J. Nucl. Mater.* 233–237 (1996) 557.
- [8] Y. Kitsunai, H. Kurishita, T. Shibayama, M. Narui, H. Kayano, Y. Hiraoka, *J. Nucl. Mater.* 239 (1996) 253.
- [9] M. Rose, A.G. Balogh, H. Hahn, *Nucl. Instrum. and Meth.* B 127&128 (1997) 119.
- [10] T. Kuwabara, H. Kurishita, S. Ukai, M. Narui, S. Mizuta, M. Yamazaki, H. Kayano, *J. Nucl. Mater.* 258–263 (1998) 1236.
- [11] Y. Chimi, A. Iwase, N. Ishikura, M. Kobiyama, T. Inami, S. Okuda, *J. Nucl. Mater.* 297 (2001) 355.
- [12] M. Samara, P.M. Derlet, H.V. Swygenhoven, M. Victoria, *Phys. Rev. Lett.* 88 (2002) 12.
- [13] S. Ukai, M. Fujiwara, *J. Nucl. Mater.* 307–311 (2002) 749.
- [14] H. Kurishita, *Basic Studies in the Field of High-Temperature Engineering*, OECD, 2002, p. 103.
- [15] S. Kobayashi, Y. Tsuruoka, K. Nakai, H. Kurishita, *Mater. Trans.* 45 (2004) 29.
- [16] S. Kobayashi, Y. Tsuruoka, K. Nakai, H. Kurishita, *J. Nucl. Mater.* 329–333 (2004) 447.
- [17] N. Nita, R. Schaeublin, M. Victoria, *J. Nucl. Mater.* 329–333 (2004) 953.
- [18] Y. Kitsunai, H. Kurishita, T. Kuwabara, M. Narui, M. Hasegawa, T. Takida, K. Takebe, *J. Nucl. Mater.* 346 (2005) 233.
- [19] H. Kurishita, T. Kuwabara, M. Hasegawa, S. Kobayashi, K. Nakai, *J. Nucl. Mater.* 343 (2005) 318.